Statistical Field Theory of Polarizable Polymer Chains with Nonlocal Dipolar Interactions

Pratik Khandagale[1, *] Carlos Garcia-Cervera,[2, 3] Gal deBotton,[4, 5]
Timothy Breitzman,[6] Carmel Majidi,[1, 7, 8] and Kaushik Dayal[7, 1, 9]

[1]*Department of Mechanical Engineering, Carnegie Mellon University*
[2]*Mathematics Department, University of California, Santa Barbara*
[3]*BCAM, Basque Center for Applied Mathematics, E48009 Bilbao, Basque Country, Spain*
[4]*Department of Mechanical Engineering, Ben Gurion University*
[5]*Department of Biomedical Engineering, Ben Gurion University*
[6]*Air Force Research Laboratory*
[7]*Department of Civil and Environmental Engineering, Carnegie Mellon University*
[8]*Department of Materials Science and Engineering, Carnegie Mellon University*
[9]*Center for Nonlinear Analysis, Department of Mathematical Sciences, Carnegie Mellon University*
(Dated: April 3, 2024)

The electromechanical response of polymeric soft matter to applied electric fields is of fundamental scientific interest as well as relevant to technologies for sensing and actuation. Several existing theoretical and numerical approaches for polarizable polymers subject to a combined applied electric field and stretch are based on discrete monomer models. In these models, accounting for the interactions between the induced dipoles on monomers is challenging due to the nonlocality of these interactions. On the other hand, the framework of statistical field theory provides a continuous description of polymer chains that potentially enables a tractable way to account for these interactions. However, prior formulations using this framework have been restricted to the case of weak anisotropy of the monomer polarizability.

This paper formulates a general approach based in the framework of statistical field theory to account for the nonlocal nature of the dipolar interactions without any restrictions on the anisotropy or nonlinearity of the polarizability of the monomer. The approach is based on 3 key elements: (1) the statistical field theory framework, in which the discrete monomers are regularized to a continuous dipole distribution; (2) a replacement of the nonlocal dipole-dipole interactions by the local electrostatics PDE with the continuous dipole distribution as the forcing; (3) the use of a completely general relation between the polarization and the local electric field. Rather than treat the dipole-dipole interactions directly, the continuous description in the field theory enables the computationally-tractable nonlocal-to-local transformation. Further, it enables the use of a realistic statistical-mechanical ensemble wherein the average far-field applied electric field is prescribed, rather than prescribing the applied field at every point in the polymer domain.

The model is applied, using the finite element method (FEM), to study the electromechanical response of a polymer chain in the ensemble with fixed far-field applied electric field and fixed chain stretch. The nonlocal dipolar interactions are found to increase, over the case where dipole-dipole interactions are neglected, the magnitudes of the polarization and electric field by orders of magnitude as well as significantly change their spatial distributions. Next, the effect of the relative orientation between the applied field and the chain on the local electric field and polarization is studied. The model predicts that the elastic response of the polymer chain is linear, consistent with the Gaussian approximation, and is largely unchanged by the orientation of the applied electric field, though the polarization and local electric field distributions are significantly impacted.

1. Introduction

Stimuli-responsive polymeric soft matter is central to actuators and sensors in applications such as soft robotics [1–11], stretchable electronics [12–15], energy harvesting [16–19], healthcare [20–24], and functional systems broadly [25–35]. Electro-responsive polarizable polymers such as dielectric elastomers (DEs) are naturally soft, lightweight, compliant, and can undergo large deformation under an applied electric field, making them promising candidate materials. However, there are also shortcomings with currently-available polymerics materials, e.g., they often need highly applied electric fields to achieve a meaningful level of actuation [36]. A fundamental understanding of the physics of polymers subjected to electric fields is essential to improve existing, and discover new, polarizable polymeric materials, e.g., in the case of statistical mechanics applied to soft matter flexoelectricity [37–42].

Prior Work. The physics of polarizable polymeric soft matter is governed by the polymer chain entropy, the interaction between the applied electric field and the induced dipoles, and the nonlocal dipolar interactions between the polymer segments (Fig. 1). Existing models for electro-responsive polymeric soft matter can be broadly divided into two categories: continuum based-approaches, e.g., [43–51], and statistical mechanics-based approaches, e.g., [37, 52–58].

---

* pkhandag@alumni.cmu.edu

Continuum approaches typically formulate the free energy density by coupling established rubber elasticity models to continuum electrostatics. These approaches are useful in enabling the study of electro-responsive polymers in complex and realistic geometries and boundary conditions. However, these approaches cannot provide predictive insights that are based in the response of the individual monomers.

The statistical mechanics based-approaches for polymers, on the other hand, are capable of accounting for the molecular details of the polymer chain. Statistical mechanics has been employed for several decades to study the mechanical response of polymers and their networks, e.g., [59–63]. In the context of electro-responsive polymers, the first works that applied statistical mechanics appear to be [52] and [53]. Broadly, their work derives an approximate expression for the most probable density of monomer orientations that is exact when the polymer chain is not stretched. Building on this, a statistical mechanics-based discrete monomer model for an electro-responsive polarizable polymer chain was presented in [54, 57]. Using the maximum term approximation assumption, they evaluated the most probable density of monomer orientation and the free energy of polymer chain applicable at large stretches. Although these theoretical approaches for electro-responsive polymers provide valuable insights, they all ignore the nonlocal dipolar interactions; they only model the interaction between the applied electric field and the induced dipoles. A key reason for this limitation is that these approaches all use a discrete description of the polymer chain, and it is computationally very expensive to account for all pairs of interactions.

In contrast, a statistical field theoretic formulation [64–66] for polarizable polymer chains in an external electric field was presented in [67] that accounts for the dipolar interactions. A key feature of the field theoretic approach is that the polymer is described as a continuous — rather than discrete — object, enabling the replacement of dipole-dipole interaction sums by integrals [68–70]. However, the formulation in [67] is limited to the setting of weak anisotropy of the polymer polarizability. Also, in the field theoretic formulation, it is challenging to account for realistic electrical boundary conditions, i.e., typically the statistical mechanics ensemble assumes that the applied field is given at every point, rather than only the far-field or average value which is more realistic.
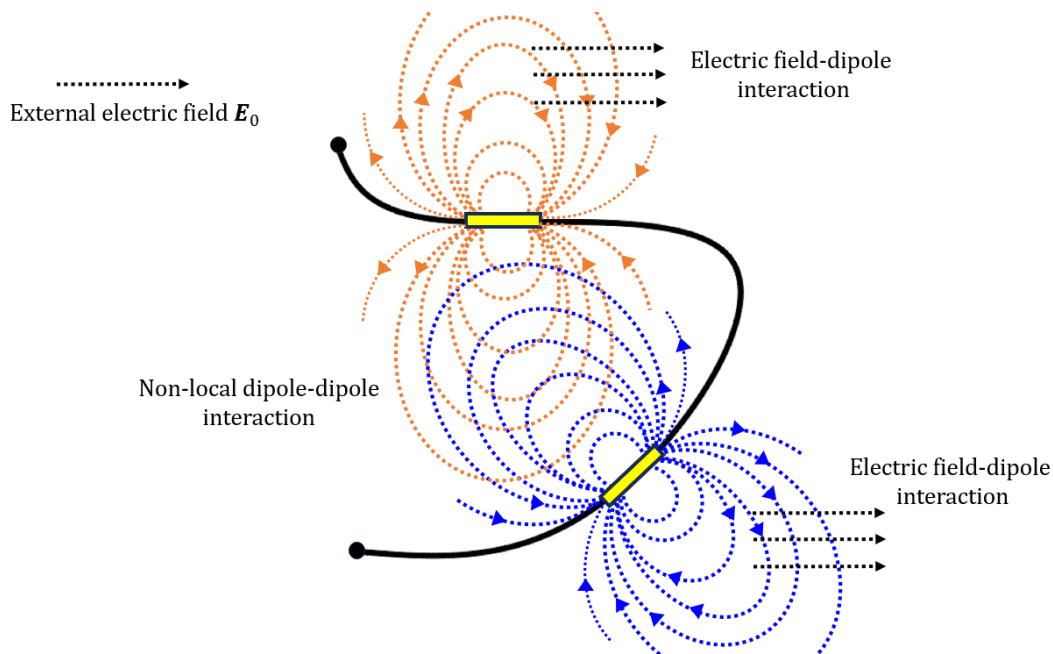

Figure 1. A polarizable polymer chain in an externally-applied far-field electric field E_0 induces dipoles in the polymer segments. The dipole-dipole interactions are long range — they decay as the inverse third power of the distance — and lead to nonlocal effects that cannot be truncated without very large error [71]. These, in turn, affect the configuration of the chain and the mechanical response. We show in this paper that neglecting the dipole-dipole interactions and only accounting for the applied field-dipole interactions, as in prior work, leads to large errors.

Contributions of This Work. To overcome the limitations of the existing models for polarizable polymeric soft matter, we have developed a statistical field theoretic framework for polarizable polymer chains that enables us to account for the nonlocal dipole-dipole interactions among the polymer segments. The approach is based on three elements.

First, the statistical field theory framework, in which the polymer chain is regularized to a continuous description. We model the polarizable flexible polymer chain using a worm-like chain (WLC) model with field-induced dipoles along the length of the chain. The continuous description enables us to avoid treating individual interactions between discrete dipoles, but instead as a tractable continuous polarization distribution.

Second, the continuous polarization description enables us to replace the nonlocal dipole-dipole interactions — an integral operation — by the local electrostatics partial differential equation (PDE) which uses instead the interaction with the local electric field set up the dipoles. To compute the effective bound charge, we introduce a polarization operator for a polymer chain, and derive an expression for the thermodynamically-averaged induced polarization.

Third, we use a completely general dielectric response function that relates the induced polarization to the local electric field. While we use a linear anisotropic relation between the polarization and the electric field for the numerical calculations, the method is directly applicable to general nonlinear response functions. Further, the dielectric response is necessarily nonlinear in the orientation to satisfy frame invariance. These elements provide a self-consistent field theoretic formulation to obtain the properties of the polymer chain — such as segment density, polarization distribution, and local electric field distribution around the polymer chain — under an externally applied electric field.

A significant aspect of our formulation is that we apply the external electric field only on the boundary of the spatial domain that includes the polymer chain as well as free space. This corresponds to a thermodynamic ensemble with specified far-field or average applied electric field [54], which is realistic in terms of experimental configurations. The local electric field is obtained self-consistently through solving for the electrostatic equation that accounts for the polarization distribution. By using the finite element method (FEM) with an unstructured discretization, we are able to efficiently solve by refining the mesh around the polymer chain where variations are large and keeping it coarse in the free space away from the chain.

The FEM implementation is applied to study the electromechanical response of a polymer chain in the ensemble with fixed far-field applied electric field and fixed chain stretch. We find that the nonlocal dipolar interactions are found to increase, over the case where dipole-dipole interactions are neglected, the magnitudes of the polarization and electric field by orders of magnitude as well as change significantly their spatial distributions. Next, we study the effect of the relative orientation between the applied field and the chain on the local electric field and polarization. When the applied electric field is aligned with the chain end-to-end vector, the larger values of the polarization and electric field are primarily concentrated near the constrained chain ends. In contrast, when the applied field is orthogonal to the chain end-to-end vector, the larger values of the polarization and electric field are distributed along the chain. However, we observe that despite these differences in the polarization and local field, the elastic response of the chain is linear and largely unchanged by the different orientations of the applied electric field.

Organization. Section 2 presents our approach; Section 3 presents the numerical method; and Section 4 presents results from our calculations.

2. Formulation

This section presents the formulation of the framework for a polarizable polymer chain under a far-field applied electric field. First, we summarize the standard self-consistent statistical field theoretic description of the polymer chain, following [66]. Next, we introduce the polarization operator and its thermodynamic average for the polarizable polymer chain, and describe the coupling between electrostatics and polymer chain description.

2.A. Self-Consistent Statistical Field Theory Description of a Polymer Chain

We use a worm-like chain (WLC) model in this paper with a small but nonzero value for the persistence length. The chain has N coarse-grained polarizable polymer segments, each with length a; $L_c = aN$ is the total contour length of the chain. The persistence length is denoted by λ, i.e., the distance along the polymer chain contour over which the orientational correlations decay. The ratio λ/L_c determines the flexibility of the chain: $\lambda/L_c \ll 1$ gives a very flexible polymer chain, whereas $\lambda/L_c \gg 1$ gives a rigid rod-like polymer chain. To model a flexible polymer chain in this work, we use $\lambda/L_c = 10^{-3}$.

A coarse-grained configuration of the polymer chain is represented as a continuous 3-d space curve $\boldsymbol{r}(s)$ in Figure 2, where s is the chain contour coordinate that is non-dimensionalized with chain contour length L_c such that $0 \leq s \leq 1$. The position and orientation of the chain segment with contour coordinate s are given by $\boldsymbol{x} = \boldsymbol{r}(s)$ and $\boldsymbol{u} = \dfrac{1}{L_c}\dfrac{\mathrm{d}\boldsymbol{r}}{\mathrm{d}s}$, respectively. The chain is assumed to be inextensible, hence $\boldsymbol{u}$ is a unit vector. The position and orientation at the ends of the chain are denoted $\boldsymbol{x}^0$ and $\boldsymbol{u}^0$ at $s = 0$ and $\boldsymbol{x}^1$ and $\boldsymbol{u}^1$ at $s = 1$.

The fundamental statistical mechanics quantity is the partition function, $Q[w]$, which has the expression:

$$Q[w] = \frac{1}{4\pi V} \int \mathrm{d}\boldsymbol{x} \int \mathrm{d}\boldsymbol{u}\, q(\boldsymbol{x}, \boldsymbol{u}, \boldsymbol{x}^0, \boldsymbol{u}^0, s) q^*(\boldsymbol{x}, -\boldsymbol{u}, \boldsymbol{x}^1, \boldsymbol{u}^1, 1 - s), \tag{2.1}$$

where $w(\boldsymbol{x}, \boldsymbol{u})$ is the potential of the external field, originating in the interaction between the induced dipole on the polymer segment and the local electric field and whose form is given in (2.13); $q(\boldsymbol{x}, \boldsymbol{u}, \boldsymbol{x}^0, \boldsymbol{u}^0, s)$ and $q^*(\boldsymbol{x}, -\boldsymbol{u}, \boldsymbol{x}^1, \boldsymbol{u}^1, 1 - s)$ are the partial partition functions of the chain for the two chain fragments, one from 0 to s and the other from 1 to s, respectively (Fig. 2); and $V = Na^2$ is the volume of the polymer chain in 2-d (we would use $V = Na^3$ for 3-d). The domain of integration is over the spatial domain in $\boldsymbol{x}$ and over the unit sphere in $\boldsymbol{u}$.
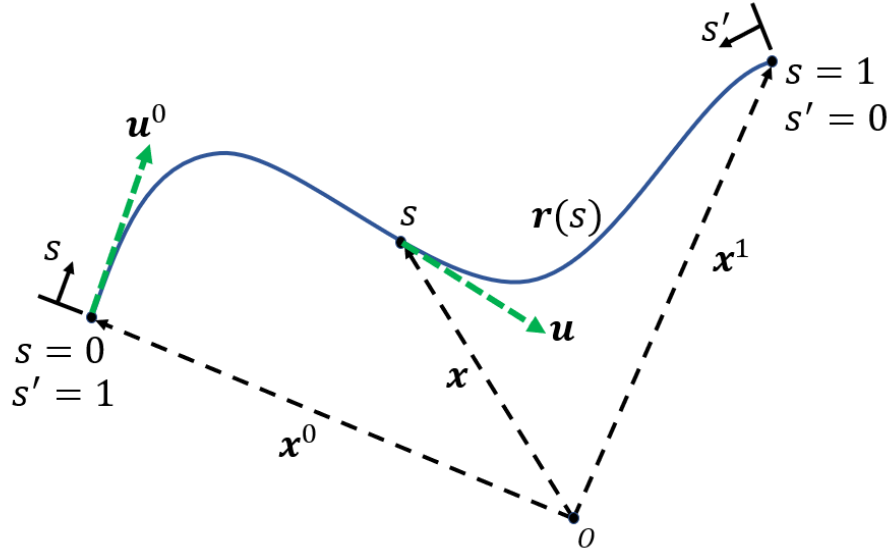
Figure 2. Kinematic quantities used to describe the polymer chain.

The partial partition functions q and q^* are obtained by solving the PDEs below [66]:

$$\frac{\partial q}{\partial s} = -w(\boldsymbol{x}, \boldsymbol{u})q - L_c \boldsymbol{u} \cdot \nabla_{\boldsymbol{x}} q + \frac{L_c}{2\lambda} \nabla_{\boldsymbol{u}}^2 q \tag{2.2}$$

$$\frac{\partial q^*}{\partial s'} = -w(\boldsymbol{x}, \boldsymbol{u})q^* - L_c \boldsymbol{u} \cdot \nabla_{\boldsymbol{x}} q^* + \frac{L_c}{2\lambda} \nabla_{\boldsymbol{u}}^2 q^* \tag{2.3}$$

where $s' = 1 - s$ varies along the chain contour in the opposite sense as s (Fig. 2).

The corresponding initial conditions are:

$$q(\boldsymbol{x}, \boldsymbol{u}, \boldsymbol{x}^0, \boldsymbol{u}^0, s)\Big|_{s=0} = V\,\delta(\boldsymbol{x} - \boldsymbol{x}^0). \tag{2.4}$$

$$q^*(\boldsymbol{x}, -\boldsymbol{u}, \boldsymbol{x}^1, \boldsymbol{u}^1, s')\Big|_{s'=0} = V\,\delta(\boldsymbol{x} - \boldsymbol{x}^1) \tag{2.5}$$

The initial conditions in (2.4) and (2.5) specify the physical constraint that the ends of the chain are fixed at $\boldsymbol{x}^0$ and $\boldsymbol{x}^1$. We do not constrain the chain orientations at the ends.

The linear PDEs in (2.2) and (2.3) are Fokker–Planck equations that govern the propagation of correlations in segment position and orientation for a worm-like polymer chain under an external field $w(\boldsymbol{x}, \boldsymbol{u})$. This system of PDEs is derived using a recursive relation based on the Markov property of the polymer chain partition function. Physically, these PDE imply that the partition function for a chain fragment from 0 to $s + \Delta s$ can be composed of two contributions: first, the partition function for the chain from 0 to s, and second, the partition function for a small additional chain segment between s and $s + \Delta s$. The partition function for this additional segment is then written, using a Boltzmann weight, in terms of the energy that consists of a quadratic contribution from chain bending and the energy due to the external field w. Taking the limit $\Delta s \to 0$ leads to the system of PDE; for the details of the derivation, we refer to Section 2.5 in [66].

The first term on the right sides of (2.2) and (2.3) relate to the external field acting on the polymer chain. The operator $\nabla_{\boldsymbol{u}}^2$ in the third term on the right side is the rotational diffusion operator that generates diffusive motion on the unit sphere.

In general, by using the appropriate form for the functional dependence of $w(\boldsymbol{x}, \boldsymbol{u})$ on $\boldsymbol{u}$, these equations can be used to describe the interaction between worm-like polymer chains with a broad class of external potentials, including electric and magnetic fields [66]. Examples include polymer chains with induced or permanent electric or magnetic dipoles along the polymer backbone, and anisotropic potential fields that can model liquid crystalline behavior. In this work, we use $w(\boldsymbol{x}, \boldsymbol{u})$ to model the electrostatic energy of the dielectric polymer chain due to induced electric dipoles in the polymer segments in an externally applied electric field.

2.B. Spatial Dipole Distribution

The density operator $\hat{\rho}(\boldsymbol{x}, \boldsymbol{u})$ for the WLC is defined as [66]:

$$\hat{\rho}(\boldsymbol{x}, \boldsymbol{u}) := \int\limits_0^1 \mathrm{d}s\, \delta(\boldsymbol{x} - \boldsymbol{r}(s))\delta\left(\boldsymbol{u} - \frac{1}{L_c}\boldsymbol{r}'(s)\right)\delta(|\boldsymbol{u}| - 1), \tag{2.6}$$

The Dirac measures build in the kinematic definitions of $\boldsymbol{x}$ and $\boldsymbol{u}$ as constraints. The thermodynamically-averaged segment density, $\langle\hat{\rho}(\boldsymbol{x}, \boldsymbol{u})\rangle$, is then obtained as [66]:

$$\langle\hat{\rho}(\boldsymbol{x}, \boldsymbol{u})\rangle = \frac{1}{4\pi V Q[w]} \int\limits_0^1 \mathrm{d}s\, q(\boldsymbol{x}, \boldsymbol{u}, \boldsymbol{x}^0, \boldsymbol{u}^0, s)q^*(\boldsymbol{x}, -\boldsymbol{u}, \boldsymbol{x}^1, \boldsymbol{u}^1, 1 - s). \tag{2.7}$$

where $\langle\cdot\rangle$ corresponds to the statistical average performed over all possible conformations of the polymer chain.

Next, we introduce the polarization operator $\hat{\boldsymbol{p}}(\boldsymbol{x}, \boldsymbol{u})$ as:

$$\hat{\boldsymbol{p}}(\boldsymbol{x}, \boldsymbol{u}) := 4\pi V \int\limits_0^1 \mathrm{d}s\, \boldsymbol{p}_{seg}(\boldsymbol{x}, \boldsymbol{u})\, \delta(\boldsymbol{x} - \boldsymbol{r}(s))\delta\left(\boldsymbol{u} - \frac{1}{L_c}\boldsymbol{r}'(s)\right)\delta(|\boldsymbol{u}| - 1), \tag{2.8}$$

where $\boldsymbol{p}_{seg}(\boldsymbol{x}, \boldsymbol{u})$ is the polarization response function, i.e., the induced polarization at the point $(\boldsymbol{x}, \boldsymbol{u})$ in configuration space.

Defining $\langle\hat{\boldsymbol{p}}(\boldsymbol{x}, \boldsymbol{u})\rangle$ as the thermodynamically-averaged polarization of the polymer segment at $(\boldsymbol{x}, \boldsymbol{u})$ in configuration space, we write:

$$\begin{aligned} \langle\hat{\boldsymbol{p}}(\boldsymbol{x}, \boldsymbol{u})\rangle &= \left\langle 4\pi V \int\limits_0^1 \mathrm{d}s\, \boldsymbol{p}_{seg}(\boldsymbol{x}, \boldsymbol{u})\, \delta(\boldsymbol{x} - \boldsymbol{r}(s))\delta\left(\boldsymbol{u} - \frac{1}{L_c}\boldsymbol{r}'(s)\right)\delta(|\boldsymbol{u}| - 1) \right\rangle \\ &= 4\pi V \boldsymbol{p}_{seg}(\boldsymbol{x}, \boldsymbol{u}) \left\langle \int\limits_0^1 \mathrm{d}s\, \delta(\boldsymbol{x} - \boldsymbol{r}(s))\delta\left(\boldsymbol{u} - \frac{1}{L_c}\boldsymbol{r}'(s)\right)\delta(|\boldsymbol{u}| - 1) \right\rangle \\ &= 4\pi V \boldsymbol{p}_{seg}(\boldsymbol{x}, \boldsymbol{u})\langle\hat{\rho}(\boldsymbol{x}, \boldsymbol{u})\rangle, \quad \text{using (2.6) and (2.7).} \end{aligned} \tag{2.9}$$

We define $\boldsymbol{p}(\boldsymbol{x})$, the polarization at the spatial location $\boldsymbol{x}$, as the average over $\boldsymbol{u}$ at the location $\boldsymbol{x}$:

$$\boldsymbol{p}(\boldsymbol{x}) := \frac{1}{4\pi} \int \mathrm{d}\boldsymbol{u}\, \langle\hat{\boldsymbol{p}}(\boldsymbol{x}, \boldsymbol{u})\rangle = V \int \mathrm{d}\boldsymbol{u}\, \boldsymbol{p}_{seg}(\boldsymbol{x}, \boldsymbol{u})\langle\hat{\rho}(\boldsymbol{x}, \boldsymbol{u})\rangle \tag{2.10}$$

This final quantity $\boldsymbol{p}(\boldsymbol{x})$ will appear in the electrostatic equation in the bound charge density.

2.C. Electrostatics

We next obtain the electric field through the local electrostatics PDE, which is tractable numerically since the charge distribution described through $\boldsymbol{p}(\boldsymbol{x})$ does not involve singular dipole distributions. This also lets us directly apply realistic boundary conditions — i.e., specified potential on the boundary of the domain, corresponding to a given far-field applied electric field — without having to compute the Greens function for a given geometry. As shown in the Appendix of [54], this ensemble is equivalent to prescribing the average field over the domain. The interior field within the domain is a superposition of the electrostatic interaction between the applied field and the induced dipole response of the polymer segments as well as the nonlocal dipole-dipole interactions among the induced dipoles. The usual electrostatics PDE accounts automatically for all of these interactions.

We start from the electrostatic equation for the electrostatic potential $\phi(\boldsymbol{x})$:

$$-\epsilon_0 \nabla^2 \phi(\boldsymbol{x}) = -\operatorname{div} \boldsymbol{p} \text{ on } \Omega, \quad \text{given } \phi(\boldsymbol{x}) = -\boldsymbol{E}_0 \cdot \boldsymbol{x} \text{ on } \partial\Omega \tag{2.11}$$

where $\boldsymbol{p}$ is obtained from (2.10); $-\operatorname{div} \boldsymbol{p}$ is the bound charge density; $\boldsymbol{E}_0$ is the given average electric field; and Ω is the region of space with boundary $\partial\Omega$ over which we solve the electrostatic problem.

The electric field $\boldsymbol{E}(\boldsymbol{x})$ is related to $\phi(\boldsymbol{x})$ through the classical relation:

$$\boldsymbol{E}(\boldsymbol{x}) = -\nabla\phi(\boldsymbol{x}). \tag{2.12}$$

In turn, the field $w(\boldsymbol{x}, \boldsymbol{u})$ is related to $\boldsymbol{E}(\boldsymbol{x})$ as [66]:

$$w(\boldsymbol{x}, \boldsymbol{u}) = -\frac{4\pi V}{2k_B T} \boldsymbol{p}_{seg}(\boldsymbol{x}, \boldsymbol{u}) \cdot \boldsymbol{E}(\boldsymbol{x}) \tag{2.13}$$

2.D. Monomer Dipole Response

We assume that the monomers that compose the chain have a dielectric response that is linear in the electric field[1]. However, the response is necessarily nonlinear in the orientation $\boldsymbol{u}$ to satisfy rotation invariance of the monomer.

We define the polarization response of a segment of the polymer chain as:

$$\boldsymbol{p}_{seg}(\boldsymbol{x}, \boldsymbol{u}) := \epsilon_0 \boldsymbol{\beta}(\boldsymbol{u}) \boldsymbol{E}(\boldsymbol{x}). \tag{2.14}$$

where $\boldsymbol{\beta}$ is related to the molecular polarizability tensor of the chain segment, and depends on the orientation of the chain segment $\boldsymbol{u}$. We model the polarizability tensor $\boldsymbol{\beta}$ as transversely isotropic [52, 53] with the expression:

$$\boldsymbol{\beta}(\boldsymbol{u}) = \beta_{\parallel} \boldsymbol{u} \otimes \boldsymbol{u} + \beta_{\perp} (\boldsymbol{I} - \boldsymbol{u} \otimes \boldsymbol{u}). \tag{2.15}$$

where $\beta_{\parallel}$ and $\beta_{\perp}$ are the polarizabilities of the segment along the segment orientation and transverse to the segment orientation, respectively.

2.E. Model Summary

The external field $w(\boldsymbol{x}, \boldsymbol{u})$ connects to the PDEs for the partial partition functions q and q^* in (2.2) and (2.3). The solutions for q and q^* in turn relate to the partition function $Q[w]$ and average segment density $\langle \hat{\rho}(\boldsymbol{x}, \boldsymbol{u}) \rangle$ using (2.1) and (2.7), respectively. Finally, to close the loop, the polarization, $\boldsymbol{p}(\boldsymbol{x})$, is related by (2.10) to $Q[w]$, $\langle \hat{\rho}(\boldsymbol{x}, \boldsymbol{u}) \rangle$, and $\boldsymbol{p}_{seg}$.

3. Numerical Method

3.A. Self-consistent Iteration

Algorithm 1 Self-consistent iterative algorithm to compute the equilibrium properties of a polymer chain

---

while $\Delta Q > \epsilon = 10^{-3}$ **do**

    Compute $\boldsymbol{p}(\boldsymbol{x}) = V \int \mathrm{d}\boldsymbol{u}\, \boldsymbol{p}_{seg}(\boldsymbol{x}, \boldsymbol{u}) \langle \hat{\rho}(\boldsymbol{x}, \boldsymbol{u}) \rangle$ $\triangleright$ $\boldsymbol{p}_{seg}(\boldsymbol{x}, \boldsymbol{u}) = \epsilon_0 \boldsymbol{\beta}(\boldsymbol{u}) \boldsymbol{E}(\boldsymbol{x})$

    Solve for $\phi(\boldsymbol{x})$: $\nabla^2 \phi(\boldsymbol{x}) = \dfrac{1}{\epsilon_0} \operatorname{div} \boldsymbol{p}(\boldsymbol{x})$,   given $\phi(\boldsymbol{x}) = -\boldsymbol{E}_0 \cdot \boldsymbol{x}$ on $\partial\Omega$

    Compute $\boldsymbol{E}(\boldsymbol{x}) = -\nabla\phi(\boldsymbol{x})$

    Compute $w(\boldsymbol{x}, \boldsymbol{u}) = -\dfrac{4\pi V}{2k_B T} \left[\epsilon_0 \boldsymbol{\beta}(\boldsymbol{u}) \boldsymbol{E}(\boldsymbol{x}) \right] \cdot \boldsymbol{E}(\boldsymbol{x})$

    Compute q and q^*, by solving (2.2) and (2.3), respectively

    Compute $Q[w]$ and $\langle \hat{\rho}(\boldsymbol{x}, \boldsymbol{u}) \rangle$, using (2.1) and (2.7), respectively

end while

Outputs: $\boldsymbol{E}^{eq}(\boldsymbol{x}), Q^{eq}, \langle \hat{\rho}(\boldsymbol{x}, \boldsymbol{u}) \rangle^{eq}, \boldsymbol{p}^{eq}(\boldsymbol{x})$

Algorithm 1 shows the iterative procedure in the proposed self-consistent field theory formulation to obtain the equilibrium properties of a polarizable polymer chain.

To initialize, i.e., guess the electric field for the initial step, we simply use $\phi(\boldsymbol{x}) = -\boldsymbol{E}_0 \cdot \boldsymbol{x}$, and use this to compute $\boldsymbol{p}$ from (2.14). To continue the numerical iteration from step n to step $n + 1$, we use $\boldsymbol{p}^n(\boldsymbol{x})$, the polarization at iteration step n, to obtain the electric potential at the next iteration step, $\phi^{n+1}(\boldsymbol{x})$, using:

$$\nabla^2 \phi^{n+1}(\boldsymbol{x}) = \frac{1}{\epsilon_0} \operatorname{div} \boldsymbol{p}^n(\boldsymbol{x}), \quad \text{given } \phi^{n+1}(\boldsymbol{x}) = -\boldsymbol{E}_0 \cdot \boldsymbol{x} \text{ on } \partial\Omega \tag{3.1}$$

$\phi^{n+1}(\boldsymbol{x})$ is used to obtain $w^{n+1}(\boldsymbol{x}, \boldsymbol{u})$ using (2.12) and (2.13). Using $w^{n+1}(\boldsymbol{x}, \boldsymbol{u})$, we again solve (2.2) and (2.3) to compute $Q[w^{n+1}]$ and $\langle \hat{\rho}(\boldsymbol{x}, \boldsymbol{u}) \rangle^{n+1}$ using (2.1) and (2.7), respectively. This in turn lets us compute $\boldsymbol{p}^{n+1}(\boldsymbol{x})$ using (2.9) and (2.10), which is used in the equation above to continue the iteration. The self-consistent iteration procedure is continued until the energy term $-k_B T \log Q$ has converged, which we check by using the change in Q across successive iterations.

---

[1] While we use a dielectric response that is linear in the electric field for this paper to perform explicit numerical calculations, it is equally easy to incorporate more general nonlinear responses.

3.B. Finite Element Formulation

We use FEM to solve the PDEs (2.2) and (2.3) for the partial partition functions as in [72]. We use FEniCS, an open-source FEM framework, for the numerical implementation [73, 74]. We work in 2 spatial dimensions (i.e., $\boldsymbol{x} = (x_1, x_2) \in \Omega \subset \mathbb{R}^2$) and restrict the unit orientation vector to the unit circle (i.e., it can be represented as $\boldsymbol{u} = (\cos\phi, \sin\phi)$, where $\phi \in [0, 2\pi)$). The configuration space in $(\boldsymbol{x}, \boldsymbol{u})$ is 3-dimensional, enabling us to use standard FEM meshing and shape functions.

In terms of $q(x_1, x_2, \phi, s)$, we can rewrite (2.2) as:

$$\frac{\partial q}{\partial s} = -wq - L_c \left(\cos\phi \frac{\partial q}{\partial x_1} + \sin\phi \frac{\partial q}{\partial x_2} \right) + \frac{L_c}{2\lambda} \left(\frac{\partial^2 q}{\partial \phi^2} \right), \tag{3.2}$$

The contour coordinate s is treated as a time-like variable. Derivatives with respect to s in (2.2) and (2.3) are approximated using a Crank-Nicolson finite difference method. We discretize in s using a uniform discretization with 100 steps along the chain contour. We can then write:

$$\frac{q^{i+1} - q^i}{\Delta s} = \frac{f^{i+1} + f^i}{2}, \quad \text{with } f^i = -wq^i - L_c \left(\cos\phi \frac{\partial q^i}{\partial x_1} + \sin\phi \frac{\partial q^i}{\partial x_2} \right) + \frac{L_c}{2\lambda} \left(\frac{\partial^2 q^i}{\partial \phi^2} \right) \tag{3.3}$$

where the superscripts i and $i+1$ represent the discretized quantities along s.

The domain in configuration space is discretized using first-order Lagrange family finite elements. We use a mesh with 20×40 finite elements to discretize in $\boldsymbol{x}$ and 30 finite elements to discretize in ϕ, which is sufficiently refined that the quantities of interest are independent of the mesh. The spatial mesh is finer around the chain ends, and the Dirac delta functions in (2.4) and (2.5) are approximated as peaked Gaussians. The mesh is uniform in the $\boldsymbol{u}$ discretization.

Following the usual FEM procedure, we first multiply (3.3) by a test function $v(x_1, x_2, \phi)$; second, integrate over $\boldsymbol{x}$ and $\boldsymbol{u}$; third, use integration-by-parts and the divergence theorem to convert the second derivatives $\dfrac{\partial^2 q}{\partial \phi^2}$ to a product of first derivatives; and, fourth, eliminate the boundary terms using the assumed Neumann boundary condition in (x_1, x_2, ϕ) to get the FEM weak form:

$$\int\limits_{\tilde{\boldsymbol{x}}, \phi} \left(q^{i+1}v + \frac{\Delta s}{2} wq^{i+1}v + \frac{\Delta s}{2} \cos\phi \frac{\partial q^{i+1}}{\partial \tilde{x}_1} v + \frac{\Delta s}{2} \sin\phi \frac{\partial q^{i+1}}{\partial \tilde{x}_2} v + \frac{L_c \Delta s}{4\lambda} \frac{\partial q^{i+1}}{\partial \phi} \frac{\partial v}{\partial \phi} \right)$$

$$= \int\limits_{\tilde{\boldsymbol{x}}, \phi} \left(q^i v - \frac{\Delta s}{2} wq^i v - \frac{\Delta s}{2} \cos\phi \frac{\partial q^i}{\partial \tilde{x}_1} v - \frac{\Delta s}{2} \sin\phi \frac{\partial q^i}{\partial \tilde{x}_2} v - \frac{L_c \Delta s}{4\lambda} \frac{\partial q^i}{\partial \phi} \frac{\partial v}{\partial \phi} \right), \tag{3.4}$$

where $\tilde{\boldsymbol{x}} = (\tilde{x}_1, \tilde{x}_2) = \left(\dfrac{x_1}{L_c}, \dfrac{x_2}{L_c} \right)$ is the nondimensional spatial coordinate.

4. Results and Discussion

In this section, we apply the model to examine the effect of dipole-dipole interactions; specifically, we compare the electric field and dipole distributions with and without accounting for dipole interactions. Then, we examine the effect of the orientation of the applied electric field, relative to the chain orientation, on the elastic response, the electric field, and the dipole distribution.

Various quantities are either nondimensionalized or rescaled, and will then be denoted by an overhead tilde $\tilde{\cdot}$. The chain is assumed to have $N = 100$ polymer segments, each having length of $a = L_c/N$. The length scales in the problem are nondimensionalized by chain contour length L_c. The computational domain is chosen to be $-0.1 \le \tilde{x}_1 \le 0.1, -0.2 \le \tilde{x}_2 \le 0.2$.

The electric field and polarization are both rescaled by dividing by $\left(\sqrt{\dfrac{2k_B T}{L_c^3}} \right)$, i.e., $\tilde{\boldsymbol{E}} = \dfrac{\boldsymbol{E}}{\sqrt{\frac{2k_B T}{L_c^3}}}$ and $\tilde{\boldsymbol{p}} = \dfrac{\boldsymbol{p}}{\sqrt{\frac{2k_B T}{L_c^3}}}$. For the polarizability tensor, we use $\beta_\parallel = 1$ and $\beta_\perp = 0.5$ following [52]. The angle between the applied electric field $\boldsymbol{E}_0$ with $\hat{\boldsymbol{e}}_1$ is denoted by $\theta_{\boldsymbol{E}_0}$.

4.A. Field and Dipole Distributions: Comparing with and without Dipole-dipole Interaction

We fix the chain end-to-end vector length to $1.5aN^{1/2}$ by fixing the chain ends at $\pm 0.075\, \boldsymbol{e}_2$ as shown in Figure 3(b). We apply a far-field electric field $\tilde{\boldsymbol{E}}_0 = \hat{\boldsymbol{e}}_2$ by using the appropriate electric potential on the boundaries of the computational domain.

Figure 3 shows the electric field, chain segment density, and polarization for the baseline case when the dipole-dipole interactions are neglected. We observe that the average segment density of the chain is highest at the constrained ends, and largely concentrated along the chain end-to-end vector. We also observe that the induced dipoles are essentially all oriented along $\tilde{\boldsymbol{E}}_0$.

Figure 4 shows a direct comparison of the polarization, $\tilde{\boldsymbol{p}}$, obtained without and with the dipole-dipole interactions for the extreme cases of the relative orientation between the applied field and the chain orientation. We observe that the polarization with
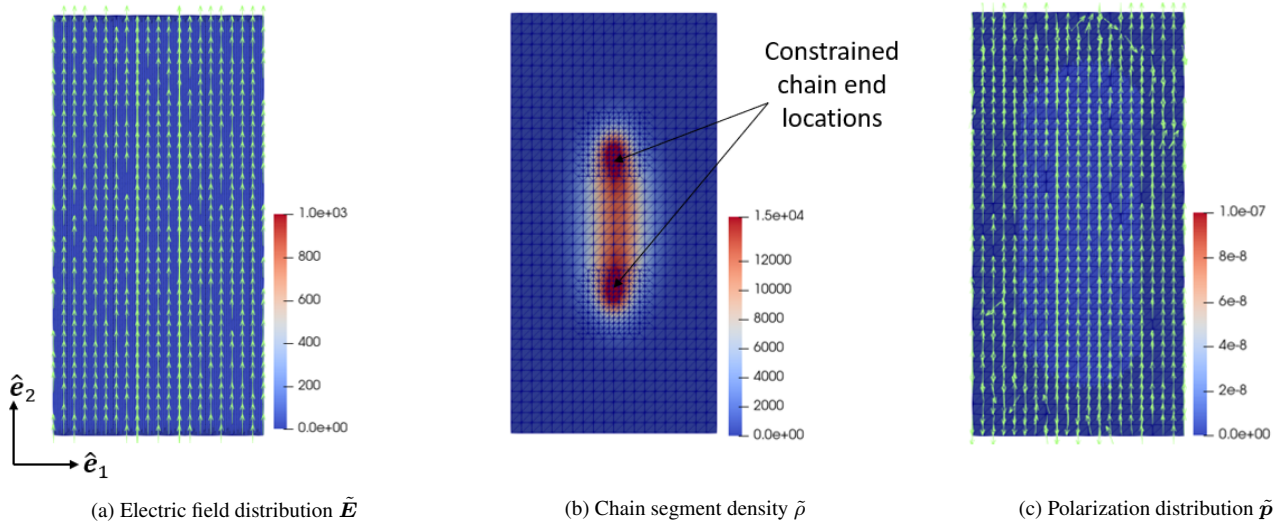
(a) Electric field distribution $\tilde{\boldsymbol{E}}$

(b) Chain segment density $\tilde{\rho}$

(c) Polarization distribution $\tilde{\boldsymbol{p}}$

Figure 3. The baseline case with dipole-dipole interactions neglected, with externally applied electric field $\tilde{\boldsymbol{E}}_0 = \hat{\boldsymbol{e}}_2$. The arrows show the direction of the vector field, and the background color shows the magnitude. (a) The electric field distribution $\tilde{\boldsymbol{E}}$, which is constant in space and equal to $\tilde{\boldsymbol{E}}_0$, as expected. (b) The chain segment density $\tilde{\rho}$. (c) The polarization distribution $\tilde{\boldsymbol{p}}$. Both the electric field and polarization distributions are close to zero on the scale of the plot, which is chosen to allow comparison with the results when dipole-dipole interactions are included.
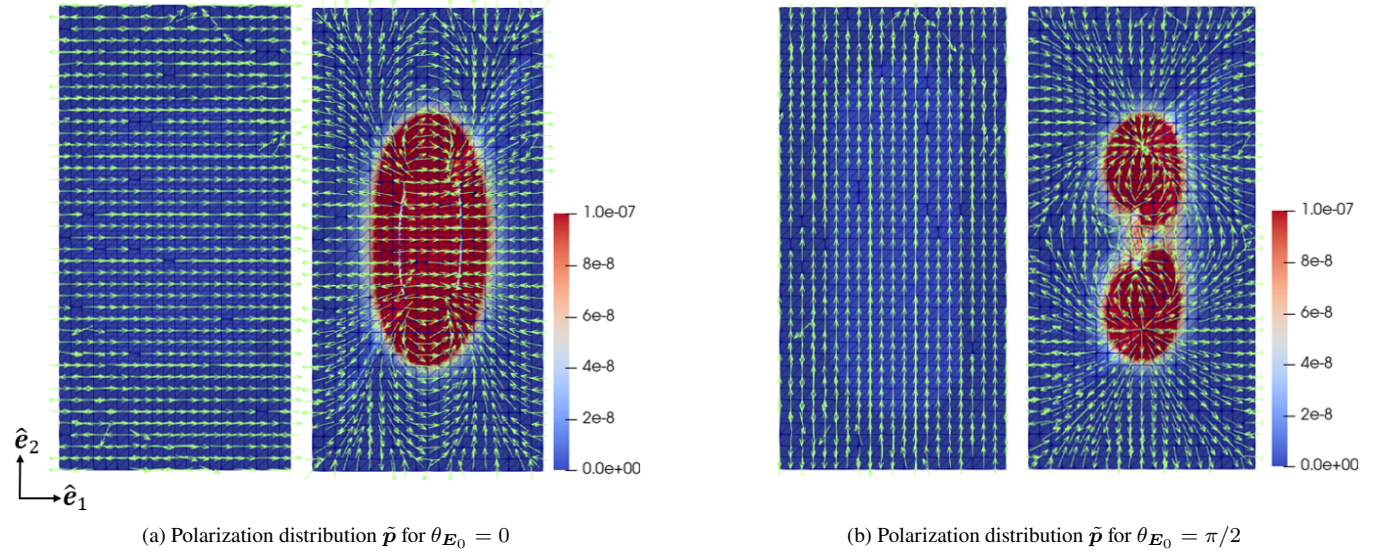

(a) Polarization distribution $\tilde{\boldsymbol{p}}$ for $\theta_{\boldsymbol{E}_0} = 0$

(b) Polarization distribution $\tilde{\boldsymbol{p}}$ for $\theta_{\boldsymbol{E}_0} = \pi/2$

Figure 4. Comparison of the polarization distribution $\tilde{\boldsymbol{p}}$, comparing without and with accounting for dipole-dipole interactions for different orientations of the applied electric field (a) $\theta_{\boldsymbol{E}_0} = 0$, and (b) $\theta_{\boldsymbol{E}_0} = \pi/2$, both with $|\tilde{\boldsymbol{E}}_0| = 1$. In both (a) and (b), the left panel is without accounting for the interactions and the right panel is with accounting for the interactions. The polarization is at least one order of magnitude larger when dipole-dipole interactions are accounted for. The arrows show the direction of the vector field, and the background color shows the magnitude.

the interactions considered is at least an order of magnitude higher than the case that neglects the interactions. Further, when the interactions are not considered, essentially all of the dipoles are oriented along $\tilde{\boldsymbol{E}}_0$, whereas there are much more complex dipole distributions when the interactions are considered. When $\tilde{\boldsymbol{E}}_0$ is aligned with the chain end-to-end vector, the polarization is largely concentrated around the chain ends. However, when $\tilde{\boldsymbol{E}}_0$ is orthogonal to the chain end-to-end vector, the polarization is relatively uniformly distributed along the chain.

We conclude that the dipole-dipole interactions not only increase the polarization by orders of magnitude, but also changes the

distribution, and depends strongly on the relative orientation of the applied electric field.

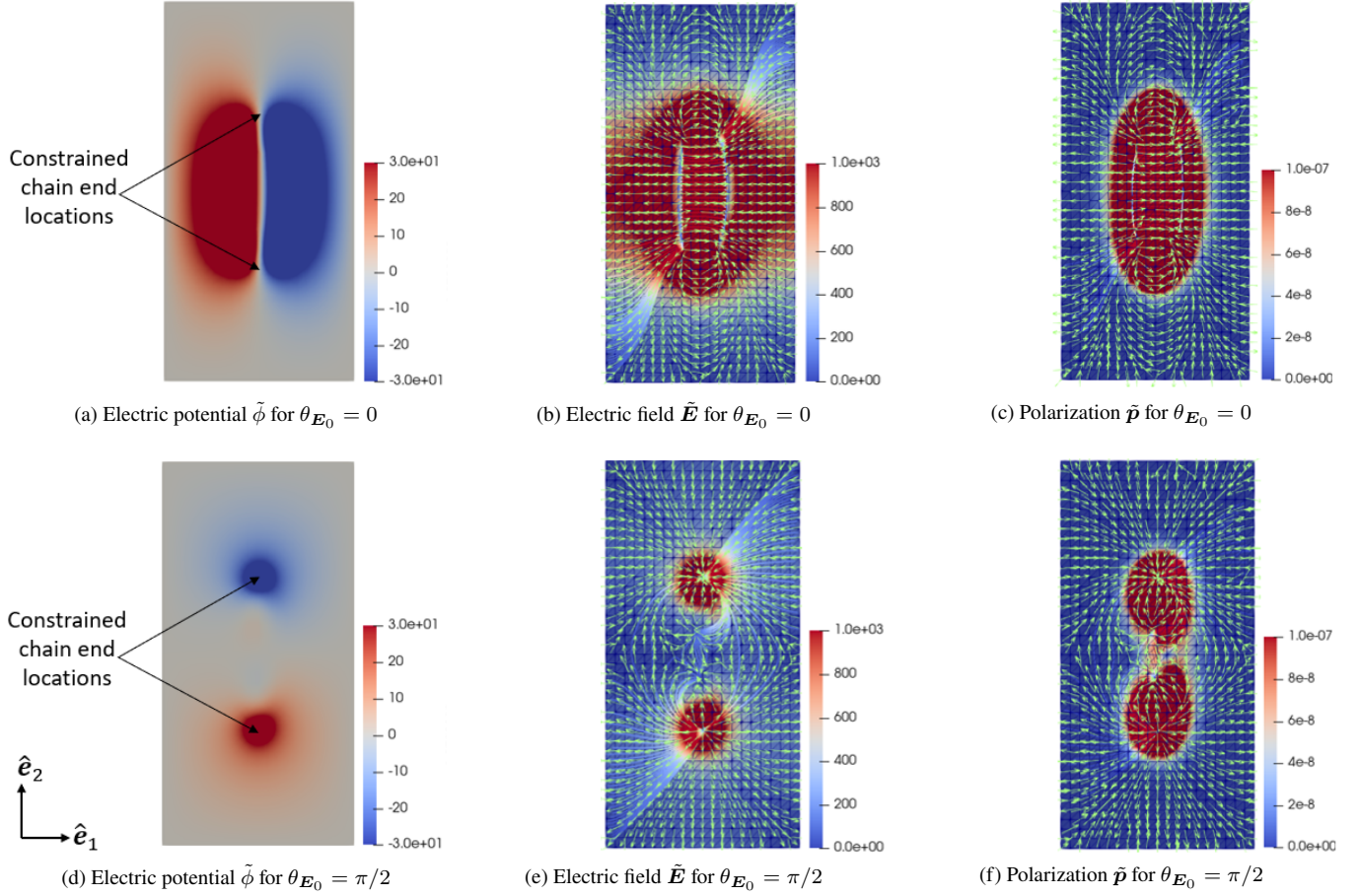## 4.B. Effect of the Orientation of the Electric Field Relative to the Chain

(a) Electric potential $\tilde{\phi}$ for $\theta_{\boldsymbol{E}_0} = 0$

(b) Electric field $\tilde{\boldsymbol{E}}$ for $\theta_{\boldsymbol{E}_0} = 0$

(c) Polarization $\tilde{\boldsymbol{p}}$ for $\theta_{\boldsymbol{E}_0} = 0$

(d) Electric potential $\tilde{\phi}$ for $\theta_{\boldsymbol{E}_0} = \pi/2$

(e) Electric field $\tilde{\boldsymbol{E}}$ for $\theta_{\boldsymbol{E}_0} = \pi/2$

(f) Polarization $\tilde{\boldsymbol{p}}$ for $\theta_{\boldsymbol{E}_0} = \pi/2$

Figure 5. Effect of orientation $\theta_{\boldsymbol{E}_0}$ of the applied electric field $\tilde{\boldsymbol{E}}_0$, with full accounting of the dipole-dipole interactions. We use $|\tilde{\boldsymbol{E}}_0(\boldsymbol{x})| = 1$. (a), (d) plot the electric potential; (b), (e) plot the electric field; and (c), (f) plot the polarization, for $\theta_{\boldsymbol{E}_0} = 0$ and $\theta_{\boldsymbol{E}_0} = \pi/2$ respectively. The arrows show the direction of the vector field, and the background color shows the magnitude.

Next, we study the effect of the orientation of the applied electric field on the properties of the polymer chain. As in the earlier section, we fix the chain ends and fix the magnitude of the applied electric field $|\tilde{\boldsymbol{E}}_0| = 1$, and study the effect of the field being orthogonal to the chain orientation compared to being aligned parallel to the chain orientation.

Figure 5 shows the electric potential, the electric field, and the polarization for $\theta_{\boldsymbol{E}_0} = 0$ and $\theta_{\boldsymbol{E}_0} = 0\pi/2$. When the applied electric field is orthogonal to the chain end-to-end vector ($\theta_{\boldsymbol{E}_0} = 0$), we observe that the dipole distribution is approximately uniformly distributed along the chain. However, when the applied electric field is aligned with the chain end-to-end vector ($\theta_{\boldsymbol{E}_0} = \pi/2$), the dipole distribution is primarily concentrated near the chain ends. The electric field distribution follows from the electric potential. Further, we observe that when the applied electric field is orthogonal to the chain end-to-end vector, the electric field is roughly uniformly distributed along the chain. However, when the applied electric field is aligned with the chain end-to-end vector, the electric field is largely concentrated near the chain ends. We also observe that the local strength of the electric potential, the electric field, and the polarization is higher when the applied electric field is orthogonal to the chain end-to-end vector as compared to when it is aligned.

4.C. Elastic Response

To study the effect of chain stretch, we vary the length of the chain end-to-end vector, denoted L. The total free energy of the polymer chain at equilibrium, F, is obtained as [75]:

$$F = -k_B T \log Q[w] - \frac{k_B T}{2} \int \mathrm{d}\boldsymbol{x} \, \mathrm{d}\boldsymbol{u} \, w(\boldsymbol{x}, \boldsymbol{u}) \langle \hat{\rho}(\boldsymbol{x}, \boldsymbol{u}) \rangle, \tag{4.1}$$
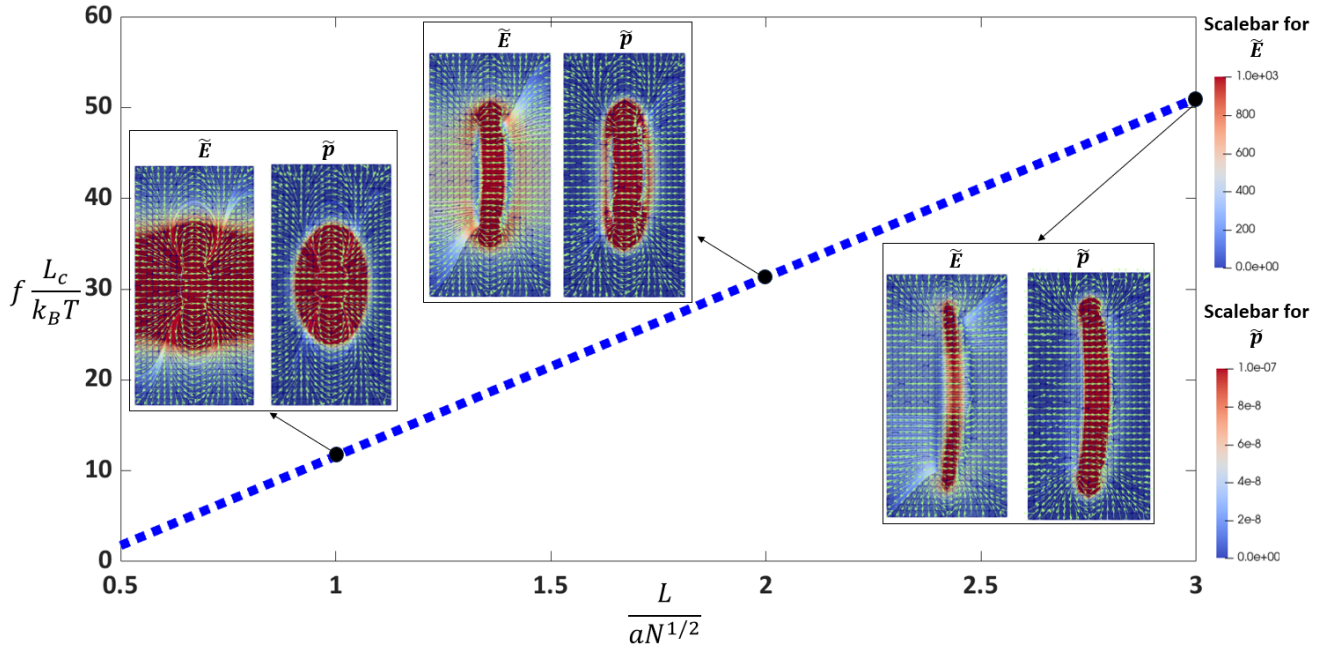
Figure 6. Elastic response (force against stretch) of the polymer chain for $\theta_{E_0} = 0$. The insets show the electric field $\widetilde{E}$ and polarization $\tilde{p}$ for $L = aN^{1/2}, 2aN^{1/2}, 3aN^{1/2}$. The arrows show the direction of the vector field, and the background color shows the magnitude.
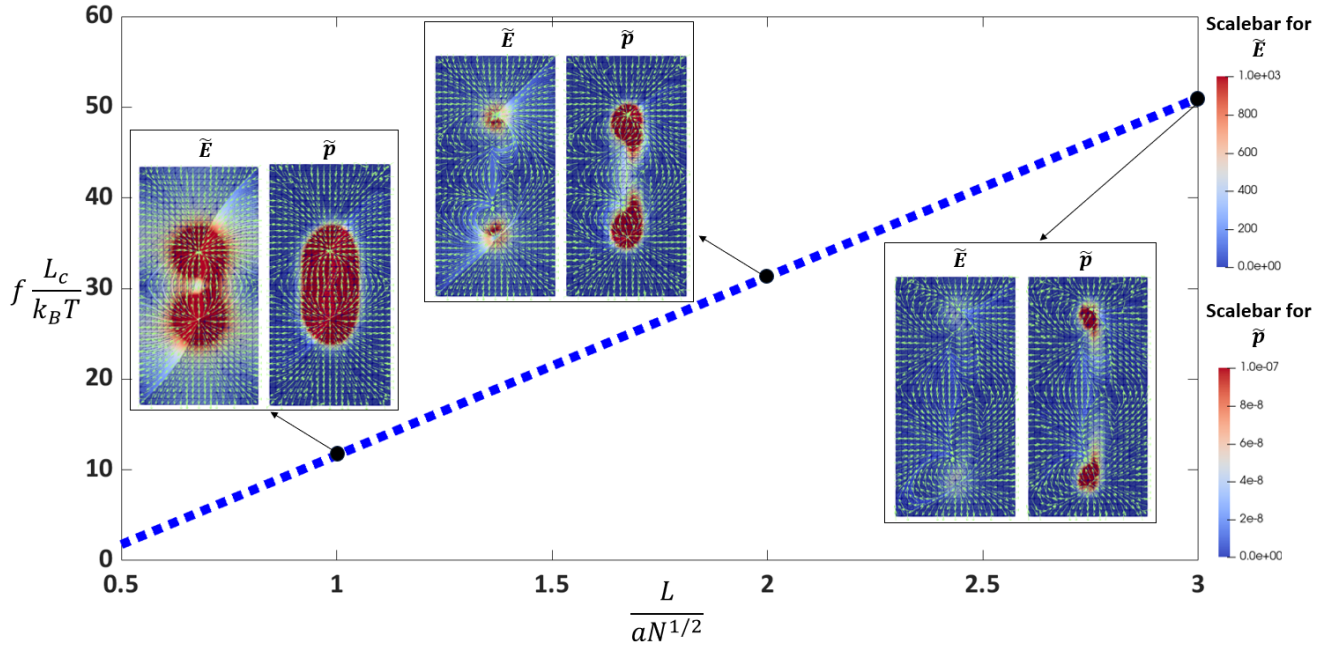

Figure 7. Elastic response (force against stretch) of the polymer chain for $\theta_{E_0} = \pi/2$. The insets show the electric field $\widetilde{E}$ and polarization $\tilde{p}$ for $L = aN^{1/2}, 2aN^{1/2}, 3aN^{1/2}$. The arrows show the direction of the vector field, and the background color shows the magnitude.

The first term is the free energy of the non-interacting polymer chain in the external field $w(\boldsymbol{x}, \boldsymbol{u})$, which double counts the electrical energy due to dipole-dipole interactions. The second term in (4.1) corrects for this double counting. We define the elastic force in the polymer chains by $f := \dfrac{\partial F}{\partial L}$.

Figures 6 and 7 show the elastic force as a function of L for the applied electric field orthogonal and parallel to the chain orientation respectively. The insets in the figures show the electric field $\widetilde{E}$ and polarization $\tilde{p}$. We observe that the elastic response is linear, which is consistent with the Gaussian nature of the polymer chain, even with the applied electric field at different

orientations. Further, the elastic force response is essentially unchanged even when we change the orientation of the applied electric field. However, the distributions of the electric field and polarization change very significantly with the direction of the applied electric field. When the applied electric field is orthogonal to the chain end-to-end vector ($\theta_{E_0} = 0$, Fig. 6), we observe that as the chain is stretched, the distributions of the electric field and polarization remain roughly uniformly distributed along the chain, but are increasingly concentrated along the chain end-to-end vector with increasing stretch. However, when the applied electric field is aligned with the chain end-to-end vector ($\theta_{E_0} = \pi/2$, Fig. 7), the electric field and the polarization are primarily concentrated near the chain ends, with the concentration changing with increasing stretch.

5.   Concluding Remarks

We have developed a statistical field theory framework for polarizable polymer chains that overcomes key limitations of existing approaches in accounting for the nonlocal dipole-dipole interactions between polymer segments. Our approach is applicable to general nonlinear polarization-electric field responses, by reformulating the nonlocal dipole-dipole interactions through the local PDE of electrostatics. Regardless of the nonlinearity of the polarization-field response, the PDE constraint is linear and directly amenable to efficient numerical methods, such as boundary element methods that can account for unbounded domains [76] or very efficient Fourier methods [77]. Our approach also enables the use of a more realistic ensemble that corresponds to a far-field applied electric field.

There are several possibilities for further development. An immediate direction of study is to incorporate general nonlinear polarization-electric field responses that go beyond the linear anisotropic model studied here. Another interesting direction would be to apply the framework developed here to study cross-linked polymer networks, e.g. following [78]. This can provide key physical insights into the effects of inter-chain dipole-dipole interactions on the response of electromechanical polymer networks such as dielectric elastomers under external fields. Yet another interesting possibility is to study polymers in confined settings with polarizable ambient media, which have been shown in other contexts to lead to unusual effects, e.g. [79, 80]. Further, by including excluded volume interactions, it is possible to study the interplay between repulsive excluded volume interactions and attractive dipole-dipole interactions to tailor the functional properties of polymeric soft matter. Furthermore, an important aspect that we have not accounted for in our formulation is the role of fluctuations; recent developments in the statistical field theory provide tools to make progress in this direction [81]. Finally, the dipole response can be generalized to account for screening, rapid variations of the electric field, and so on [67]. In principle, these can be accounted for in our model — screening by using the screened Poisson equation, for instance, and using gradients of the electric field in the monomer dipole response to account for quadrupole and higher moments — but it is important to demonstrate these in practice.

[1] Paul Brochu and Qibing Pei. Dielectric elastomers for actuators and artificial muscles. *Electroactivity in polymeric materials*, pages 1–56, 2012.

[2] Kwang J Kim and Satoshi Tadokoro. Electroactive polymers for robotic applications. *Artificial Muscles and Sensors*, 23:291, 2007.

[3] Samuel Rosset, Benjamin M O'Brien, Todd Gisby, Daniel Xu, Herbert R Shea, and Iain A Anderson. Self-sensing dielectric elastomer actuators in closed-loop operation. *Smart Materials and Structures*, 22(10):104018, 2013.

[4] Edouard Leroy, Ronan Hinchet, and Herbert Shea. Multimode hydraulically amplified electrostatic actuators for wearable haptics. *Advanced Materials*, 32(36):2002564, 2020.

[5] Xiaobin Ji, Xinchang Liu, Vito Cacucciolo, Matthias Imboden, Yoan Civet, Alae El Haitami, Sophie Cantin, Yves Perriard, and Herbert Shea. An autonomous untethered fast soft robotic insect driven by low-voltage dielectric elastomer actuators. *Science Robotics*, 4(37):eaaz6451, 2019.

[6] Vito Cacucciolo, Jun Shintake, Yu Kuwajima, Shingo Maeda, Dario Floreano, and Herbert Shea. Stretchable pumps for soft machines. *Nature*, 572(7770):516–519, 2019.

[7] Taylor H Ware, John S Biggins, Andreas F Shick, Mark Warner, and Timothy J White. Localized soft elasticity in liquid crystal elastomers. *Nature communications*, 7(1):1–7, 2016.

[8] Mahnoush Babaei, Junfeng Gao, Arul Clement, Kaushik Dayal, and M Ravi Shankar. Torque-dense photomechanical actuation. *Soft Matter*, 17(5):1258–1266, 2021.

[9] Jiangshui Huang, Tiefeng Li, Choon Chiang Foo, Jian Zhu, David R Clarke, and Zhigang Suo. Giant, voltage-actuated deformation of a dielectric elastomer under dead load. *Applied Physics Letters*, 100(4), 2012.

[10] Anil Erol, Saad Ahmed, Zoubeida Ounaies, and Paris von Lockette. A microstructure-based approach to modeling electrostriction that accounts for variability in spatial locations of domains. *Journal of the Mechanics and Physics of Solids*, 124:35–62, 2019.

[11] Kevin LoGrande, M Ravi Shankar, and Kaushik Dayal. A dimensionally-reduced nonlinear elasticity model for liquid crystal elastomer strips with transverse curvature. *Soft Matter*, 19(45):8764–8778, 2023.

[12] John A Rogers, Takao Someya, and Yonggang Huang. Materials and mechanics for stretchable electronics. *science*, 327(5973):1603–1607, 2010.

[13] Keun Soo Kim, Yue Zhao, Houk Jang, Sang Yoon Lee, Jong Min Kim, Kwang S Kim, Jong-Hyun Ahn, Philip Kim, Jae-Young Choi, and Byung Hee Hong. Large-scale pattern growth of graphene films for stretchable transparent electrodes. *nature*, 457(7230):706–710, 2009.

[14] Dahl-Young Khang, Hanqing Jiang, Young Huang, and John A Rogers. A stretchable form of single-crystal silicon for high-performance electronics on rubber substrates. *Science*, 311(5758):208–212, 2006.

[15] Sheng Xu, Yihui Zhang, Jiung Cho, Juhwan Lee, Xian Huang, Lin Jia, Jonathan A Fan, Yewang Su, Jessica Su, Huigang Zhang, et al. Stretchable batteries with self-similar serpentine interconnects and integrated wireless recharging systems. *Nature communications*, 4(1):1–8, 2013.

[16] Thomas G McKay, Samuel Rosset, Iain A Anderson, and Herbert Shea. Dielectric elastomer generators that stack up. *Smart Materials and Structures*, 24(1):015014, 2014.

[17] Mengdi Han, Heling Wang, Yiyuan Yang, Cunman Liang, Wubin Bai, Zheng Yan, Haibo Li, Yeguang Xue, Xinlong Wang, Banu Akar, et al. Three-dimensional piezoelectric polymer microsystems for vibrational energy harvesting, robotic interfaces and biomedical implants. *Nature Electronics*, 2(1):26–35, 2019.

[18] Alper Erturk and Daniel J Inman. *Piezoelectric energy harvesting*. John Wiley & Sons, 2011.

[19] Kewang Nan, Stephen Dongmin Kang, Kan Li, Ki Jun Yu, Feng Zhu, Juntong Wang, Alison C Dunn, Chaoqun Zhou, Zhaoqian Xie, Matthias T Agne, et al. Compliant and stretchable thermoelectric coils for energy harvesting in miniature flexible devices. *Science advances*, 4(11):eaau5849, 2018.

[20] Jean Won Kwak, Mengdi Han, Zhaoqian Xie, Ha Uk Chung, Jong Yoon Lee, Raudel Avila, Jessica Yohay, Xuexian Chen, Cunman Liang, Manish Patel, et al. Wireless sensors for continuous, multimodal measurements at the skin interface with lower limb prostheses. *Science translational medicine*, 12(574):eabc4327, 2020.

[21] Qian Zhang, Qijie Liang, and John A Rogers. Water-soluble energy harvester as a promising power solution for temporary electronic implants. *APL Materials*, 8(12):120701, 2020.

[22] Sheng Xu, Yihui Zhang, Lin Jia, Kyle E Mathewson, Kyung-In Jang, Jeonghyun Kim, Haoran Fu, Xian Huang, Pranav Chava, Renhan Wang, et al. Soft microfluidic assemblies of sensors, circuits, and radios for the skin. *Science*, 344(6179):70–74, 2014.

[23] Seung-Kyun Kang, Rory KJ Murphy, Suk-Won Hwang, Seung Min Lee, Daniel V Harburg, Neil A Krueger, Jiho Shin, Paul Gamble, Huanyu Cheng, Sooyoun Yu, et al. Bioresorbable silicon electronic sensors for the brain. *Nature*, 530(7588):71–76, 2016.

[24] Dae-Hyeong Kim, Nanshu Lu, Rui Ma, Yun-Soung Kim, Rak-Hwan Kim, Shuodao Wang, Jian Wu, Sang Min Won, Hu Tao, Ahmad Islam, et al. Epidermal electronics. *science*, 333(6044):838–843, 2011.

[25] Yang Jiao and Pinar Akcora. Understanding the role of grafted polystyrene chain conformation in assembly of magnetic nanoparticles. *Physical Review E*, 90(4):042601, 2014.

[26] Murugappan Muthukumar. *Physics of Charged Macromolecules*. Cambridge University Press, 2023.

[27] Dhriti Nepal, Jeffrey Haines, and Richard A Vaia. Polymer nanocomposites: 35 years on. *MRS Bulletin*, pages 1–11, 2023.

[28] Navid Zolfaghari, Pratik Khandagale, Michael J Ford, Kaushik Dayal, and Carmel Majidi. Network topologies dictate electromechanical coupling in liquid metal–elastomer composites. *Soft Matter*, 16(38):8818–8825, 2020.

[29] Morteza Amjadi, Ki-Uk Kyung, Inkyu Park, and Metin Sitti. Stretchable, skin-mountable, and wearable strain sensors and their potential applications: a review. *Advanced Functional Materials*, 26(11):1678–1698, 2016.

[30] Qian Deng, Liping Liu, and Pradeep Sharma. Electrets in soft materials: Nonlinearity, size effects, and giant electromechanical coupling. *Physical Review E*, 90(1):012603, 2014.

[31] Lingling Chen, Xu Yang, Binglei Wang, Shengyou Yang, Kaushik Dayal, and Pradeep Sharma. The interplay between symmetry-breaking and symmetry-preserving bifurcations in soft dielectric films and the emergence of giant electro-actuation. *Extreme Mechanics Letters*, 43:101151, 2021.

[32] Yongyi Zhao, Pratik Khandagale, and Carmel Majidi. Modeling electromechanical coupling of liquid metal embedded elastomers while accounting stochasticity in 3d percolation. *Extreme Mechanics Letters*, 48:101443, 2021.

[33] Liping Liu and Pradeep Sharma. Giant and universal magnetoelectric coupling in soft materials and concomitant ramifications for materials science and biology. *Physical Review E*, 88(4):040601, 2013.

[34] Evan Galipeau and Pedro Ponte Castañeda. A finite-strain constitutive model for magnetorheological elastomers: magnetic torques and fiber rotations. *Journal of the Mechanics and Physics of Solids*, 61(4):1065–1090, 2013.

[35] Junshi Zhang, Hualing Chen, and Dichen Li. Nonlinear dynamical model of a soft viscoelastic dielectric elastomer. *Physical Review Applied*, 8(6):064016, 2017.

[36] Yoseph Bar-Cohen. *Electroactive polymer (EAP) actuators as artificial muscles: reality, potential, and challenges*, volume 136. SPIE press, 2004.

[37] Matthew Grasinger, Kosar Mozaffari, and Pradeep Sharma. Flexoelectricity in soft elastomers and the molecular mechanisms underpinning the design and emergence of giant flexoelectricity. *Proceedings of the National Academy of Sciences*, 118(21), 2021.

[38] Yashashree Kulkarni. Fluctuations of active membranes with nonlinear curvature elasticity. *Journal of the Mechanics and Physics of Solids*, 173:105240, 2023.

[39] Rubayet Hassan, Maria Alejandra Garzon, Wei Gao, and Fatemeh Ahmadpoor. Entropic pressure on fluctuating solid membranes. *Journal of the Mechanics and Physics of Solids*, page 105523, 2023.

[40] F Ahmadpoor, Q Deng, LP Liu, and P Sharma. Apparent flexoelectricity in lipid bilayer membranes due to external charge and dipolar distributions. *Physical Review E*, 88(5):050701, 2013.

[41] Fatemeh Ahmadpoor and Pradeep Sharma. Flexoelectricity in two-dimensional crystalline and biological membranes. *Nanoscale*, 7(40):16555–16570, 2015.

[42] Matthew Zelisko, Fatemeh Ahmadpoor, Huajian Gao, and Pradeep Sharma. Determining the gaussian modulus and edge properties of 2d materials: From graphene to lipid bilayers. *Physical Review Letters*, 119(6):068002, 2017.

[43] Richard A Toupin. The elastic dielectric. *Journal of Rational Mechanics and Analysis*, 5(6):849–915, 1956.

[44] Luis Dorfmann and Ray W Ogden. *Nonlinear theory of electroelastic and magnetoelastic interactions*, volume 1. Springer, 2014.

[45] Liping Liu and Pradeep Sharma. Emergent electromechanical coupling of electrets and some exact relations—the effective properties of soft materials with embedded external charges and dipoles. *Journal of the Mechanics and Physics of Solids*, 112:1–24, 2018.

[46] Sana Krichen, Liping Liu, and Pradeep Sharma. Liquid inclusions in soft materials: Capillary effect, mechanical stiffening and enhanced electromechanical response. *Journal of the Mechanics and Physics of Solids*, 127:332–357, 2019.

[47] Xiaobao Li, Liping Liu, and Pradeep Sharma. Geometrically nonlinear deformation and the emergent behavior of polarons in soft matter. *Soft matter*, 11(41):8042–8047, 2015.

[48] Faezeh Darbaniyan, Kaushik Dayal, Liping Liu, and Pradeep Sharma. Designing soft pyroelectric and electrocaloric materials using electrets. *Soft matter*, 15(2):262–277, 2019.

[49] JW Fox and NC Goulbourne. On the dynamic electromechanical loading of dielectric elastomer membranes. *Journal of the Mechanics and Physics of Solids*, 56(8):2669–2686, 2008.

[50] Yali Li and Nakhiah C Goulbourne. Constitutive formulations for intrinsic anisotropy in soft electroelastic materials. *Scientific Reports*, 13(1):14712, 2023.

[51] Joshua Furer and Pedro Ponte Castañeda. Homogenization, macroscopic instabilities and domain formation in magnetoactive composites: Theory and applications. *Journal of the Mechanics and Physics of Solids*, 169:105081, 2022.

[52] Noy Cohen, Kaushik Dayal, and Gal deBotton. Electroelasticity of polymer networks. *Journal of the Mechanics and Physics of Solids*, 92:105–126, 2016.

[53] Noy Cohen and Gal deBotton. Electromechanical interplay in deformable dielectric elastomer networks. *Physical review letters*, 116(20):208303, 2016.

[54] Matthew Grasinger and Kaushik Dayal. Statistical mechanical analysis of the electromechanical coupling in an electrically-responsive polymer chain. *Soft Matter*, 16(27):6265–6284, 2020.

[55] Matthew Grasinger and Kaushik Dayal. Architected elastomer networks for optimal electromechanical response. *Journal of the Mechanics and Physics of Solids*, 146:104171, 2021.

[56] Matthew Grasinger, Carmel Majidi, and Kaushik Dayal. Nonlinear statistical mechanics drives intrinsic electrostriction and volumetric torque in polymer networks. *Physical Review E*, 103(4):042504, 2021.

[57] Matthew Grasinger, Kaushik Dayal, Gal deBotton, and Prashant K Purohit. Statistical mechanics of a dielectric polymer chain in the force ensemble. *Journal of the Mechanics and Physics of Solids*, 158:104658, 2022.

[58] Mikhail Itskov, Vu Ngoc Khiêm, and Sugeng Waluyo. Electroelasticity of dielectric elastomers based on molecular chain statistics. *Mathematics and Mechanics of Solids*, 24(3):862–873, 2019.

[59] Leslie Ronald George Treloar. *The physics of rubber elasticity*. Oxford University Press, USA, 1975.

[60] Werner Kuhn and Franz Grün. Statistical behavior of the single chain molecule and its relation to the statistical behavior of assemblies consisting of many chain molecules. *Journal of polymer science*, 1(3):183–199, 1946.

[61] Jerome Harris Weiner. *Statistical mechanics of elasticity*. Courier Corporation, 2012.

[62] Gilles Marckmann and Erwan Verron. Comparison of hyperelastic models for rubber-like materials. *Rubber chemistry and technology*, 79(5):835–858, 2006.

[63] Pratik Khandagale, Timothy Breitzman, Carmel Majidi, and Kaushik Dayal. Statistical field theory for nonlinear elasticity of polymer networks with excluded volume interactions. *Physical Review E*, 107(6):064501, 2023.

[64] Glenn H Fredrickson. Computational field theory of polymers: opportunities and challenges. *Soft Matter*, 3(11):1329–1334, 2007.

[65] Glenn H Fredrickson, Venkat Ganesan, and François Drolet. Field-theoretic computer simulation methods for polymers and complex fluids. *Macromolecules*, 35(1):16–39, 2002.

[66] Glenn Fredrickson. *The equilibrium theory of inhomogeneous polymers*, volume 134. Oxford University Press on Demand, 2006.

[67] Jonathan M Martin, Wei Li, Kris T Delaney, and Glenn H Fredrickson. Statistical field theory description of inhomogeneous polarizable soft matter. *The Journal of chemical physics*, 145(15):154104, 2016.

[68] Kevin Shen and Zhen-Gang Wang. Electrostatic correlations and the polyelectrolyte self energy. *The Journal of chemical physics*, 146(8), 2017.

[69] Jian Jiang, Valeriy V Ginzburg, and Zhen-Gang Wang. Density functional theory for charged fluids. *Soft Matter*, 14(28):5878–5887, 2018.

[70] Bilin Zhuang and Zhen-Gang Wang. Statistical field theory for polar fluids. *The Journal of Chemical Physics*, 149(12), 2018.

[71] Jason Marshall and Kaushik Dayal. Atomistic-to-continuum multiscale modeling with long-range electrostatic interactions in ionic solids. *Journal of the Mechanics and Physics of Solids*, 62:137–162, 2014.

[72] David M Ackerman, Kris Delaney, Glenn H Fredrickson, and Baskar Ganapathysubramanian. A finite element approach to self-consistent field theory calculations of multiblock polymers. *Journal of Computational Physics*, 331:280–296, 2017.

[73] M. S. Alnaes, J. Blechta, J. Hake, A. Johansson, B. Kehlet, A. Logg, C. Richardson, J. Ring, M. E. Rognes, and G. N. Wells. The FEniCS project version 1.5. *Archive of Numerical Software*, 3, 2015.

[74] A. Logg, K.-A. Mardal, G. N. Wells, et al. *Automated Solution of Differential Equations by the Finite Element Method*. Springer, 2012.

[75] Russell KW Spencer, Bae-Yeun Ha, and Nima Saeidi. Self-consistent field theory of chiral nematic worm-like chains. *The Journal of Chemical Physics*, 156(11), 2022.

[76] Kaushik Dayal and Kaushik Bhattacharya. A real-space non-local phase-field model of ferroelectric domain patterns in complex geometries. *Acta materialia*, 55(6):1907–1917, 2007.

[77] Xiaoyao Peng, Dhriti Nepal, and Kaushik Dayal. Effective response of heterogeneous materials using the recursive projection method. *Computer Methods in Applied Mechanics and Engineering*, 364:112946, 2020.

[78] Matthew Grasinger. Polymer networks which locally rotate to accommodate stresses, torques, and deformation. *Journal of the Mechanics and Physics of Solids*, 175:105289, 2023.

[79] Paul Robin, Nikita Kavokine, and Lydéric Bocquet. Modeling of emergent memory and voltage spiking in ionic transport through angstrom-scale slits. *Science*, 373(6555):687–691, 2021.

[80] AP Dos Santos, F Jiménez-Ángeles, A Ehlen, and M Olvera De La Cruz. Modulation of ionic conduction using polarizable surfaces. *Physical Review Research*, 5(4):043174, 2023.

[81] Ashesh Ghosh, Quinn MacPherson, Zhen-Gang Wang, and Andrew J Spakowitz. Semiflexible polymer solutions. ii. fluctuations and frank elastic constants. *The Journal of Chemical Physics*, 157(15), 2022.

[82] Pratik Dinkar Khandagale. *Statistical Field Theory for Polymer Networks and Electro-mechanical Polymers: Accounting for Nonlocal Interactions*. PhD thesis, Carnegie Mellon University, 2022.